FACTA UNIVERSITATIS
Series: **Mechanical Engineering**
https://doi.org/10.22190/FUME221126001H

Review article

PEAKFORCE QUANTITATIVE NANOMECHANICAL MAPPING FOR SURFACE ENERGY CHARACTERIZATION ON THE NANOSCALE: A MINI-REVIEW

Heebo Ha[1], Sebastian Müller[2], Roelf-Peter Baumann[2], Byungil Hwang[1]

[1]School of Integrative Engineering, Chung-Ang University, Republic of Korea
[2]Material Physics, Structures and Surfaces, RAA/OS, BASF SE, Germany

Abstract. *Surface energy characterization is important to design the fabrication process of reliable electronic devices. Surface energy is influenced by various factors such as surface functionality and morphology. Owing to the high surface-to-volume ratio, surface energy at the nanoscale can be different from that of the bulk. However, the conventional methods for characterization of surface energy such as a sessile drop or Washburn methods cannot be used for nanoscale samples, owing to the limited volume for characterization. Recently, surface energy characterization on the nanoscale using atomic force microscopy (AFM) with Peak Force-Quantitative Nanomechanical Mapping (PF-QNM) imaging mode has been proposed. The nanoscale AFM tips measure the adhesion forces at the nanoscale, which are converted into surface energy through pre-calibrated curves. Successful surface energy characterization of nanoscale metal samples using AFM with the PF-QNM method has been reported previously. This mini-review discusses the recent progress on surface energy characterization at the nanoscale using AFM with the PF-QNM method. The fundamentals of the PF-QNM mode are introduced, and the results of surface energy characterization are summarized. Consequently, the future research direction for surface energy characterization at the nanoscale is discussed.*

Key words: *Surface energy, Peak Force-quantitative nanomechanical napping, Nanoscale, Metal*

Received: November 26, 2022 / Accepted: January 11, 2023
Corresponding author: Byungil Hwang
School of Integrative Engineering, Chung-Ang University, 84 Heukseok-Ro, Dongjak-Gu, Seoul 06974, Republic of Korea
E-mail: bihwang@cau.ac.kr

1. INTRODUCTION

With the development of low-dimensional devices with unique characteristics, building a heterostructure of two-dimensional (2D) layered materials on three-dimensional (3D) materials and thin film hetero epitaxy have been widely investigated [1-3]. Integrating 2D materials with 3D materials and layer-by-layer stacking of thin films result in unprecedented physical and chemical properties, which can be used in various applications such as electronic skin [4-6], health care [7-9], diagnostic devices [10-12], and power generators [13-16]. Nevertheless, building continuous heterostructure and direct transfer of 2D materials or thin films on different substrates is challenging. Therefore, to develop reproducible and reliable exfoliation and transfer 2D materials and thins film stacking on different thin films or 3D structures, surface characterization of these materials is needed.

Despite the importance of surface characterization of materials, the conventionally adopted method to determine the surface energy involves measuring the contact angle between the liquid droplet and the solid surface interface [17-22]. This liquid droplet contact angle measurement can only measure at bulk scale or microscale owing to the inert size of the liquid droplet, thereby limiting nanoscale measurements. Moreover, unlike bulk or microscale materials, nanoscale materials show different properties owing to the high surface area to volume ratio, which implies that small changes in the surface energy at a few nanometers scale can significantly alter the property of nanomaterials. Thus, characterizing the surface energy of materials at the nanoscale is important.

There are different methods to determine surface energy by measuring the contact angle. Typically, the sessile drop method is used, which measures the contact angle of a liquid droplet on a solid surface using the Young equation [23-25],

$$\gamma_{sg} - \gamma_{sl} - \gamma_{lg} * cos\theta = 0 \tag{1}$$

where θ, γ_{sg}, γ_{sl}, and γ_{lg} are the contact angle, interfacial energy at the substrate-gas, substrate-liquid, and liquid-gas interfaces, respectively [18, 19]. In the case of solid powder, the Washburn adsorption method is used, which calculates the contact angle by measuring the weight of the solution adsorbed by the capillary phenomenon when the powder-filled cylinder is dipped into the solution; this is done using the Washburn equation,

$$cos\theta = \frac{\eta}{C\rho^2\gamma_L} * \frac{m^2}{t} \tag{2}$$

where θ, η, C, ρ, γ_L, t, m, and t are the contact angle, liquid viscosity, material constant, density, surface tension, weight, and time, respectively [26, 27]. Although these methods are effective in bulk solid materials, with a decrease in material size, methods for evaluating surface energy through contact angle become complicated and are not able to achieve the necessary resolution, especially at the nanoscale. In addition, the Washburn method cannot measure the surface energy of a single powder.

To address this challenge, recently, a new technology was proposed to characterize surface energy at the nanoscale using atomic force microscopy (AFM) with Peak Force-Quantitative Nanomechanical Mapping (PF-QNM) imaging mode [17, 28, 29]. This method obtains a calibration curve comprising a plot of adhesion forces versus contact angle/surface energy for macroscale samples; then, by coupling the adhesive force of nanoscale material measured using AFM PF-QNM with calibration curve, the surface

energy of the nanomaterials is estimated. Although several attempts have been made for surface energy characterization of nanoscale metal strips using AFM PF-QNM, further research is required for various forms of samples, such as powder, 2-D materials, and porous systems. For this, it is important to summarize as well as discuss the recent progress in the surface energy characterization technology using AFM PF-QNM. In this mini-review, the recently reported results of surface energy characterization using AFM PF-QNM are summarized. The fundamentals of the AFM PF-QNM method are introduced, where the theoretical background and the process to evaluate the surface energy on the nanoscale are presented. Our perspective on the AFM PF-QNM method is shared, which provides ideas for future research on surface energy characterization at the nanoscale using the AFM PF-QNM method.

2. SURFACE ENERGY CHARACTERIZATION USING AFM-PF-QNM METHOD

2.1 Principles of AFM PF-QNM Imaging Mode

Fig. 1a shows the schematic of the surface energy measurement process of nanoscale metals. In the first step of measurement, a calibration curve is acquired, where adhesion forces versus contact angle/surface energy of macroscale metals are plotted [28]. To achieve different hydrophobicity values, the macroscale metals were treated with several thiol SAMs. After the SAM treatment, the contact angle/surface energy and adhesion force of the macroscale metals are measured using the sessile drop method and AFM-QNM, respectively. The calibration curve is obtained by correlating the macroscale contact angle/surface energy and adhesion force. Afterward, the adhesion force of nanoscale metals is measured using AFM-QNM. Finally, the contact angle and the surface energy of nanoscale metals were extracted by substituting the adhesion force of nanoscale metals into the obtained calibration curves.

PF-QNM is a novel functioning mode of AFM that can record real-time force versus separation curves by periodical tapping of peak force on the desired area of the sample using a low frequency. The maximum vertical force that presses down the sample surface is recorded as the peak force. In the PF-QNM mode, the peak force shows a constant value since the software calculates the force between the AFM tip and the surface of samples based on the feedback reflecting the surface morphology and mechanical properties. Fig. 1b shows a plot of force versus time during one tapping cycle of the PF-QNM operation (Fig. 1d): (A) positioning the AFM tip on the surface of the sample surface at a given height and ready to touch the surface, (B) touching the sample surface with the tip and then applying pressure until amounting to the peak force, (C) withdrawing the tip from the surface of the sample, (D) entirely detaching of the tip from the surface of the sample after reaching the maximum attractive force point, which represents the adhesion force, (E) returning of the tip to its original height position. After one tapping cycle (A-E) is completed, the next tapping cycle starts all over again.

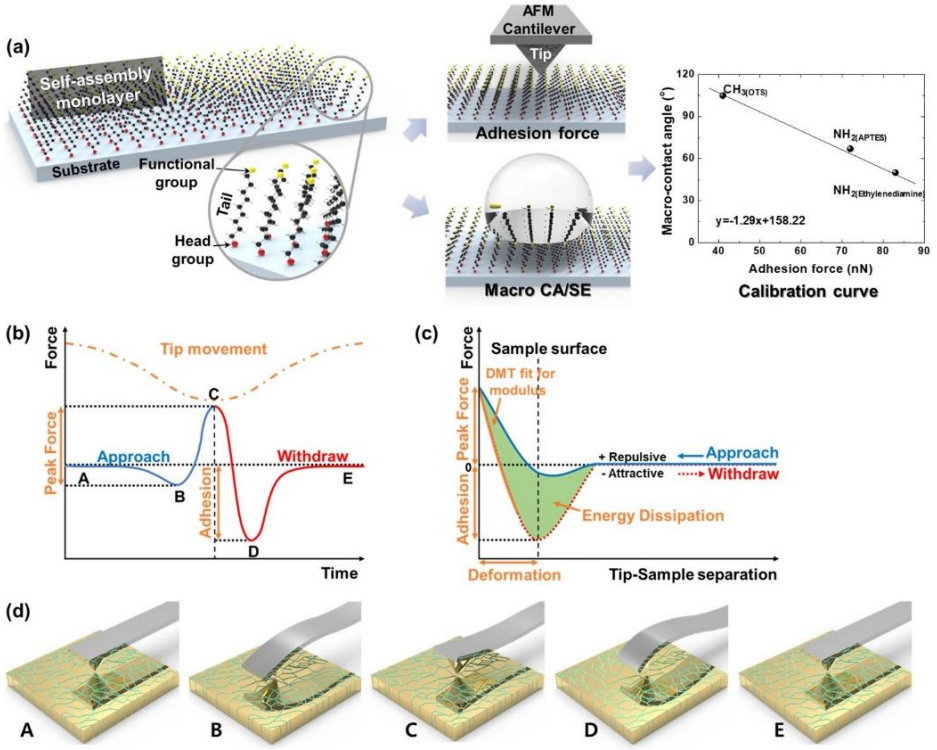

Fig. 1 (a) Schematic of the CA and SE measurement procedure for the nanoscale materials via nCA-AFM (b) Illustration of AFM PF-QNM imaging plot of force and Z-piezo/tip movement as a function of time, and (c) force curve for analyzing the material-specific properties. (d) Schematic of the AFM PF Tapping technique; cantilever oscillated below resonance, resulting in a continuous series of force-distance curves [28]. Reproduced with permission from ref. [28].

The force versus separation curve quantitatively denotes the various mechanical properties of the surface at each point, such as adhesion, Derjaguin-Muller-Toporov (DMT) modulus, and energy dissipation (Fig. 1c) [30-32]. Adhesion force is the required force to detach the AFM tip from the surface. In the force versus separation curve, the adhesion force is the force difference between the maximum attractive force point and the noncontact point. Young's modulus can be calculated with the reduced modulus, which is derived using the DMT model expressed as follows:

$$F_{interaction} = \frac{4}{3} E^* \sqrt{R(d - d_0)^3} + F_{adh} \tag{3}$$

where $F_{interaction}$ is the tip-sample force, E^* is the reduced elastic modulus of the tip and the sample, R is the tip radius, d_0 is the surface rest position, $(d - d_0)$ is the sample deformation, and F_{adh} is the adhesion force during the contact [31, 33, 34]. The Young's modulus of the sample is calculated with the reduced modulus values using the following equation:

$$E^* = \left(\frac{1-v_s^2}{E_s} + \frac{1-v_{tip}^2}{E_{tip}}\right)^{-1} \quad (4)$$

where v_s is the Poisson's ratio of the sample, v_{tip} is the Poisson's ratio of the tip, E_s is the Young's modulus of the sample, and E_{tip} is Young's modulus of the tip [31, 33, 34]. The areal gap in the curves between the approaching and withdrawing of one cycle of tapping represents the energy dissipation released during the PF-QNM imaging mode.

2.2 Surface Energy of Nanoscale Metal Strips

Park et al. characterized the surface energy of Au nano ribbons with a width of 430 nm and a thickness of 100 nm [20]. Fig. 2b shows the SEM image of Au nano ribbon tested in the study. To make a calibration curve, thiols such as 1-undecanethiol ($CH_3(CH_2)_9SH$), 11-mercapto-1-undecanol ($OH(CH_2)_{11}SH$), 11-mercaptoundecanoic acid ($COOH(CH_2)_9CH_2SH$), and 1H,1H,2H,2H-perfluorodecanethiol ($CF_3(CF_2)_7CH_2CH_2SH$), which have end groups of CF_3, CH_3, COOH, and OH, respectively, were used to modify the surface of the reference substrates. The macro contact angle and surface energy of thiol-modified substrates were characterized using the sessile drop method, which were then plotted with the adhesion forces measured for the corresponding substrates using the PF-QNM method. The calibration curves were made for the flattened Au thin film surface fabricated through the process in Fig. 2a. Fig. 2c and d shows the plots of contact angle versus adhesion forces and surface energy versus adhesion forces, respectively. The linear changes in the macro contact angle (Fig. 2c) and adhesion forces (Fig. 2d) as a function of the adhesion forces are shown with slopes of -27.53 and 16.26, respectively. Then, the adhesion forces of the Au nano ribbons were measured using the PF-QNM method, which yielded a value of ~2.31 nN. Thus, the contact angle and surface energy were estimated as 78.83° and 38.57 mN/m, respectively, by extracting the values corresponding to the adhesion force of the Au nano ribbons from the calibration curves (blue dot lines in Figs. 2c, d). These values were similar to those of bulk Au, which has a contact angle of ~74.38° and a surface energy of ~38.59 mN/m. Although this study was the first to report on the surface energy characterization for nanoscale samples using the PF-QNM method, they provided results only for a single sample, which is insufficient to understand the mechanism of surface energy change on the nanoscale.

Ha et al. investigated the effect of grain size on the surface energy of nanoscale Au thin films using the PF-QNM method [28]. To form different grain sizes, Au thin films with different thicknesses of 10, 50, and 100 nm were deposited on the SiO_2 substrates using the thermal evaporation method (Figs. 3a-c). The change in the thickness from 10 nm to 100 nm caused the increase in RMS roughness by ~0.5 nm (Figs. 3d-f), which was negligible compared to the film thickness and AFM tip radius. All the deposited film showed the identical crystallographic orientation as confirmed by X-ray diffraction (XRD) as shown in Fig. 3g. The grain sizes estimated through XRD data were 10.0, 29.0, and 41.2 nm for thicknesses of 10, 50, and 100 nm, respectively (Fig. 3h). Surface morphology and lattice constants for all the samples as shown in the high-resolution transmission electron microscopy (HRTEM) images (Figs. 3j-o), which confirmed that there was no significant distortion of microstructure during further deposition to increase the thickness of Au thin films. In addition, XPS peaks of all the samples showed the same binding energies of 87.87 and 84.20 eV as confirmed by X-ray photoelectron spectroscopy (XPS) results in Fig. 3i.

Therefore, the Au thin films deposited with different thicknesses was a suitable material system to investigate the effect of grain boundary densities on the surface energy.

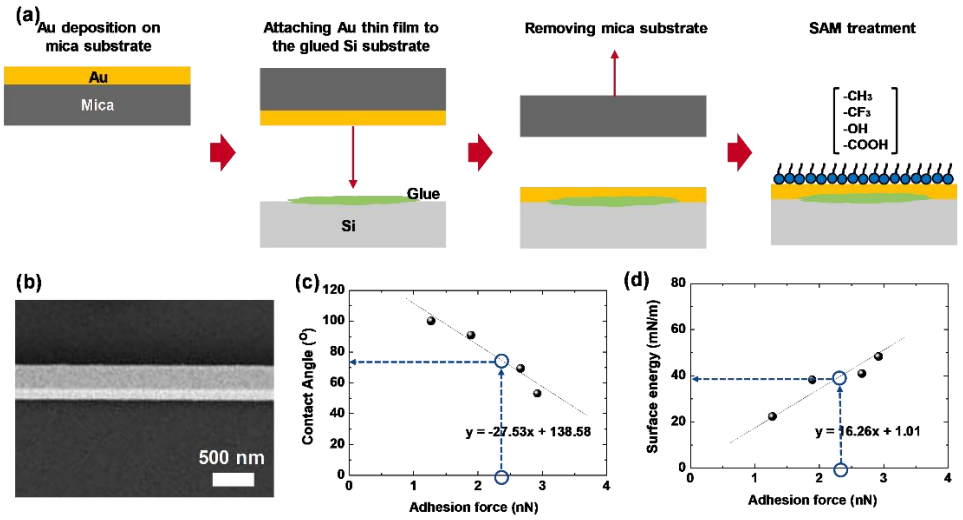

Fig. 2 (a) SEM image of Au nano ribbon. The calibration curves plotted by using the data from different thiols for evaluation of (b) contact angle and (c) surface energy of nanoscale Au ribbon [17]. Reproduced with permission from ref. [17].

To make the calibration curve, the macro contact angle and surface energy for the substrates treated with the different silanes such as N-[3-(trimethoxysilyl)propyl]ethylenediamine, (3-aminopropyl)triethoxysilane (APTES), and octyltrichlorosilane (OTS) were measured using the sessile drop method. Then, the adhesion forces for each substrate were measured using the PF-QNM method (Figs. 4e-g). Figs. 4a and b shows the calibration plots for contact angle and surface energy, respectively. The macro contact angle values linearly decreased as the measured adhesion force (F_{adh}) increased, as shown in Fig. 2c, whereas the surface energy was proportional to F_{adh}. These plots provide the equation to calculate the nano contact angle and surface energy, which are as follows:

$$\text{nCA (contact angle)} = -1.19 \times F_{adh} + 153.77 \tag{5}$$

and

$$\text{SE (surface energy)} = 0.51 \times F_{adh} + 1.86 \tag{6}$$

Once the F_{adh} values for the nanoscale samples are obtained, the values of contact angle and surface energy can be calculated using the above-mentioned equations. The adhesion forces of the Au thin films with different thicknesses, that is, grain sizes, were measured using the PF-QNM method; then, the measured values were used as input for the derived equations to evaluate the nanoscale contact angle and surface energy. Figs. 3c and d are the calculated contact angle and surface energy as a function of grain boundary density (D_{GB}), which is calculated by dividing the diameter of the AFM tip with a radius of ~125 nm with the average grain size. The adhesion force was smaller for the Au thin

films with lower D_{GB} than those with higher D_{GB}, which resulted in a linear increase in the contact angle as a function of D_{GB} (Fig. 3c). The surface energy is inversely proportional to D_{GB}, where a higher D_{GB} showed higher surface energy (Fig. 3d). Consequently, the rational equations,

$$F_{adh} = \frac{40}{D_{GB}} + 28.8 \tag{7}$$

and $$SE_{nc}\ (\text{surface energy of the nanocrystalline surface}) = \frac{21.2}{D_{GB}} + 16.0 \tag{8}$$

were derived, which indicated that the surface energy of the nanoscale metals is inversely proportional to the grain size of the samples.

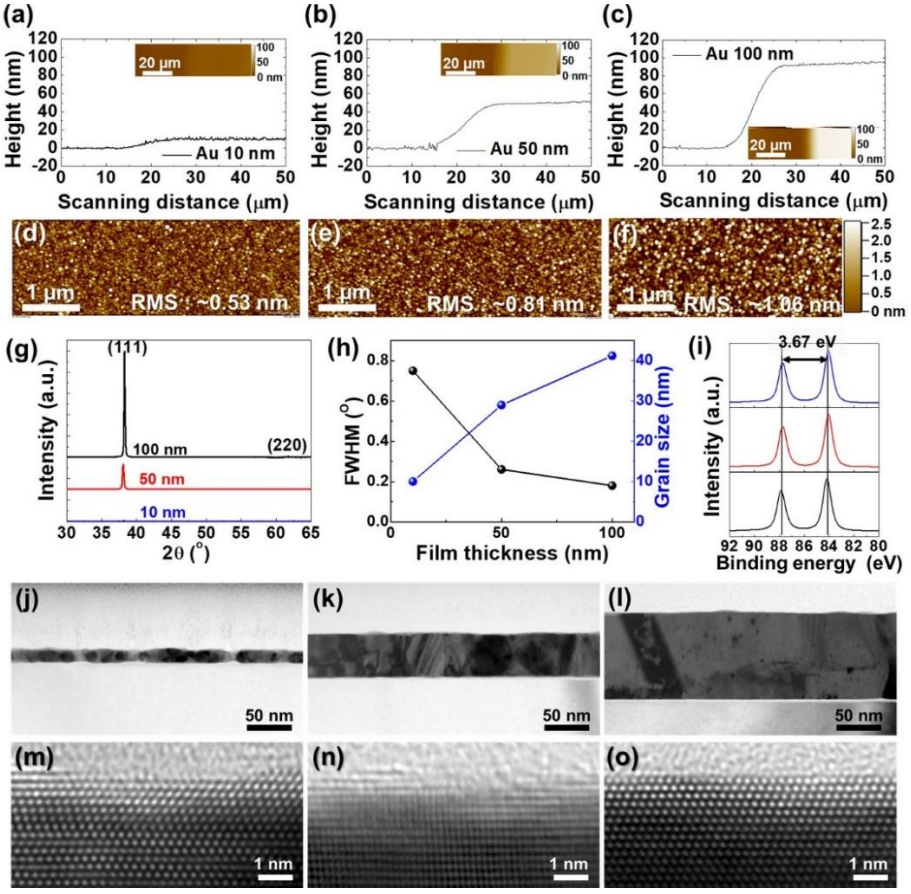

Fig. 3 (a-c) AFM topography images and profile sections on the edge of the evaporated Au layers on the SiO_2 substrate. AFM topography images of (d) 10 nm, (e) 50 nm, and (f) 100 nm thick Au layer; corresponding RMS surface roughness values are also indicated. (g) XRD pattern and (h) variation in full width at half maximum (FWHM) and GS. (i) XPS spectra results and (j-l) HRTEM images of Au films and (m-o) atom lattice with different thicknesses [28]. Reproduced with permission from ref. [28].

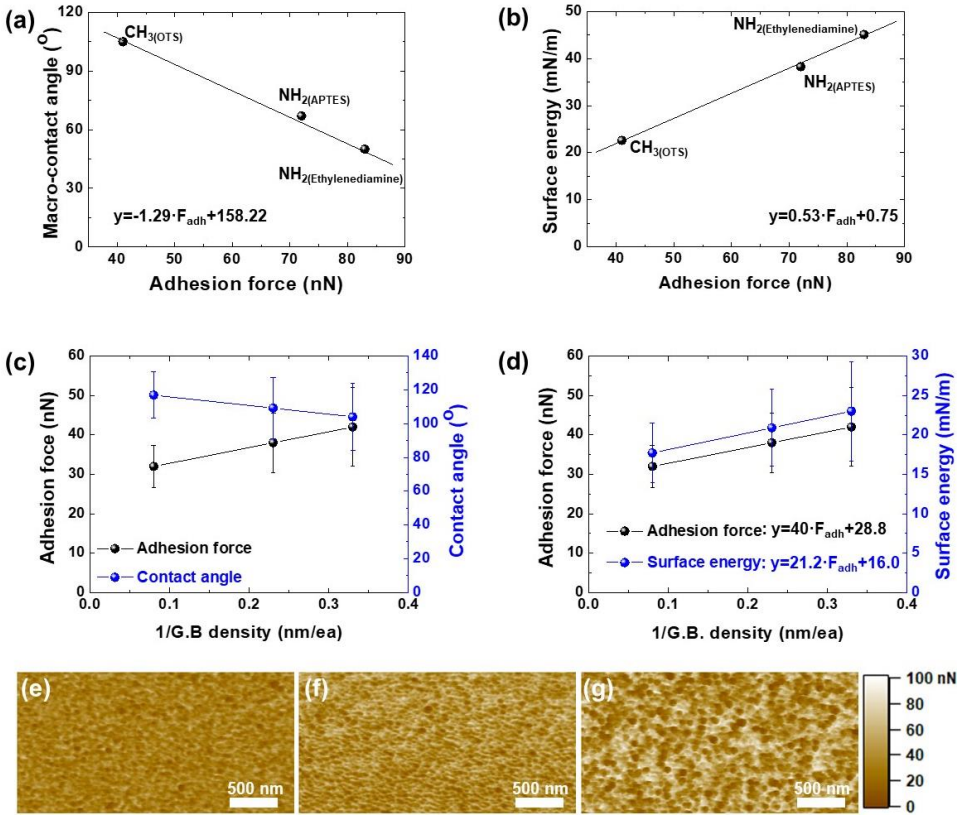

Fig. 4 Calibration plot consisting of adhesion forces from different alkyl silane self-assembled monolayers measured using the AFM PF-QNM mode versus (a) macro CA and (b) SE of SAMs evaluated using a Krüss DSA100 drop shape analyzer. Variation of nanoscale adhesion forces measured on top of 10, 50, and 100 nm thick Au layers and converted using the calibration curve into an equivalent nanoscopic (c) CA and (d) SE. Adhesion force mapping images of (e) 10 nm, (f) 50 nm, and (g) 100 nm thick Au layer [28]. Reproduced with permission from ref. [28].

In the other work by Ha et al., the effect of pattern size in nanoscale on the surface energy Au strips were investigated [29]. The thermally evaporated Au strips were manufactured on Si substrate to have thicknesses (T) of 50 nm and 100nm (Fig. 5i). The length (L) of the strips was fixed as 1000 nm while the width (W) was varied as 200 nm, 300 nm, 400 nm and 500 nm (Figs. 5a-h). The vacuum-deposition process has a great influence on the nucleation and growth of Au crystal on the Si substrate. The morphology of Au strips that corresponds to the grain size of Au and the roughness of surface was largely governed by the processing temperature, deposition rate (Å/s) and status of vacuum during the thermal evaporation step, which consequently influenced the nanoscale contact angle and surface energy. The increase in grain size of Au resulted in the higher RMS values as shown in Fig. 5j. The thinner film might cause a slightly higher density of nucleation that promotes the formation of small Au grains on the substrate. On the other

hand, the deposition time for thicker Au thin films was longer than those of thinner films that provides sufficient time for atoms to be arranged step-by-step, thereby forming larger and uniformly oriented grains.

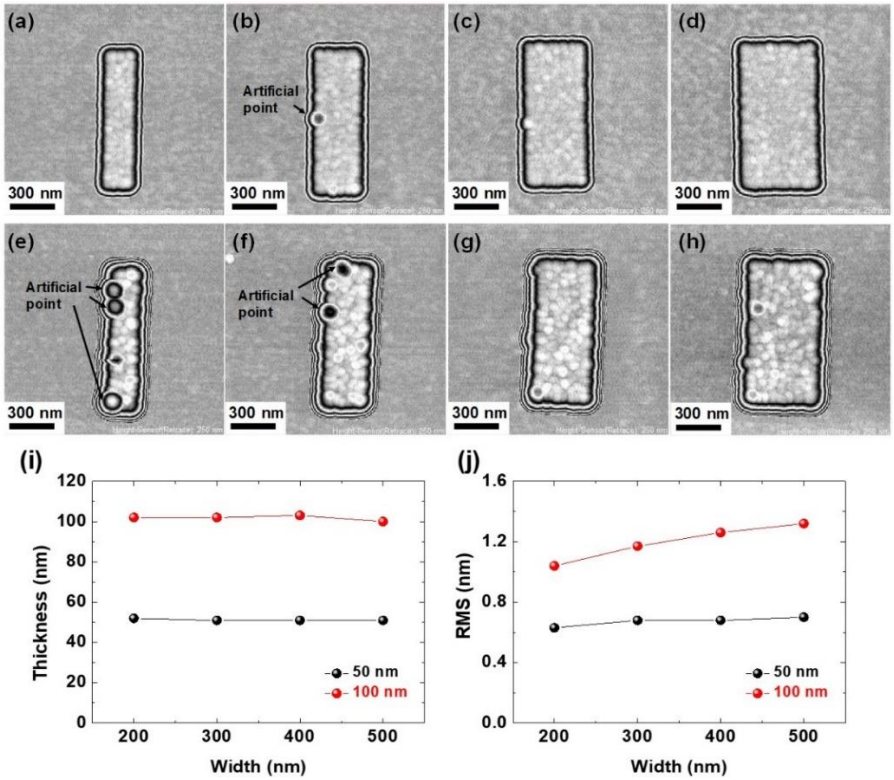

Fig. 5 AFM topography images of Au strips with thicknesses of (a-d) 50 nm and (e-f) 100 nm and widths of (a, e) 200 nm, (b, f) 300 nm, (c, g) 400 nm, and (d, h) 500 nm. (i) Thickness and (j) RMS values of Au strips with the different widths measured by AFM mapping [29]. Reproduced with permission from ref. [29].

The nano contact angle (nCA) and surface energy (SE) of the Au strips were characterized by using a AFM-PF QNM method. The calibration curves were prepared for the substrates treated with the different alkyl silanes such as Methoxy(polyethyleneoxy)-propyl]-trimethoxysilane (MPT), APTES, and OTS (Figs. 6a and b). Based on the calibration plots, the standard equations can be derived for nCA and SE as follow.

$$\text{nCA (contact angle)} = -1.29 \times F_{adh} + 158.22 \quad (9)$$

$$\text{SE (surface energy)} = 0.53 \times F_{adh} + 0.75 \quad (10)$$

Figs. 6c and d show the converted nCA and SE values for the measured adhesion forces of Au strips with different widths using the standard equation (9) and (10), respectively. The nCA and SE values showed no clear relation with the widths of Au strips in the

identical thickness, which was attributed to the similar adhesion forces. On the other hand, the change in film thickness resulted in the large difference in nCA and SE values, which was due to the increased adhesion force by the increased thickness. Therefore, it was concluded that the grain size was governing factor to determine SE of Au strips while the change in dimension in few hundreds of nanometer scale of nanoscale led to no significant change in SE of Au thin films.

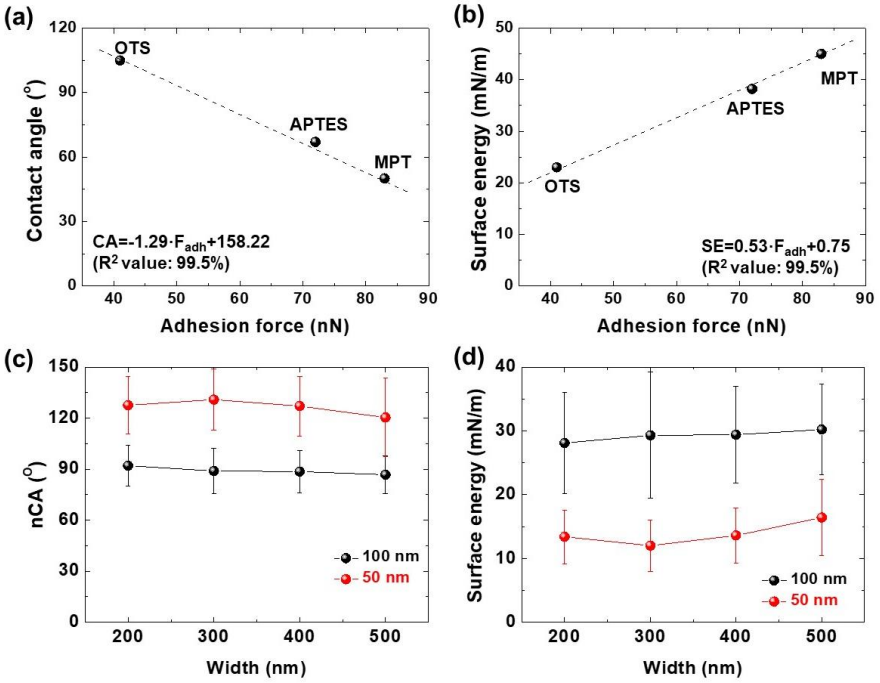

Fig. 6 Calibration plot consisting of the adhesion force from different alkyl silane self-assembled monolayers measured by AFM in PF-QNM mode versus the (a) macroscopic contact angle or (b) surface energy. (c) Translated nCA and (c) surface energy of Au strips as a function of the widths of Au strips [29]. Reproduced with permission from ref. [29].

3. CONCLUSIONS

This mini-review discusses the recent trends in the novel technology for surface energy characterization at the nanoscale using AFM PF-QNM. PF-QNM is a special function of AFM that can be used to obtain the adhesion profile throughout the scanned area. The adhesion force is created by surface characteristics such as functionalities or morphology; thus, the surface energy is correlated to the adhesion forces. By deriving the calibration curves that present the relationship between the adhesion force versus and contact angle/surface energy, the contact angle or surface energy at the nanoscale is calculated. This method can overcome the limitations of the previous surface energy characterization methods using the sessile drop method or Washburn method. Several reports demonstrated

the potential of PF-QNM for surface energy characterization at the nanoscale by successfully measuring the surface energy of Au nanoribbons and nanocrystalline Au thin films. Although these studies revealed the important relationship between the surface energy of nanoscale samples and morphology such as grain size, other factors such as roughness or defect densities are still unclear. Moreover, once the sample size further decreases to the atomic scale, even defect densities on the surface significantly influence the surface energy. Therefore, further research is required on the surface energy characterization on the atomic scale using the PF-QNM method. Furthermore, atomic simulation should be carried out simultaneously to investigate PF-QNM-based surface energy characterization. PF-QNM opened a new research area on surface energy change at the nanoscale. We hope that this mini-review encourages further studies on surface energy at the nanoscale, especially by correlating experimental characterization results and theoretical simulation evidence.

Acknowledgement: *This work was supported by a National Research Foundation of Korea (NRF) grant funded by the Korean government (MSIT) (No. NRF-2022R1F1A1063696). This research was supported by the Chung-Ang University Research Scholarship Grants in 2021.*

REFERENCES

1. Hwang, B., Kim, W., Kim, J., Lee, S., Lim, S., Kim, S., Oh, S.H., Ryu, S., Han, S.M., 2017, *Role of Graphene in Reducing Fatigue Damage in Cu/Gr Nanolayered Composite*, Nano Letters, 17(8), pp. 4740-4745.
2. Hwang, B., Han, Y., Matteini, P., 2022, *Bending Fatigue Behavior of Ag Nanowire/Cu Thin-Film Hybrid Interconnects for Wearable Electronics*, Facta Universitatis-Series Mechanical Engineering, 20(3), pp. 553-560.
3. Ha, H.-B., Lee, B.H., Qaiser, N., Seo, Y., Kim, J., Koo, J.M., Hwang, B., 2022, *Highly Reliable Anisotropic Interconnection System Fabricated Using Cu/Sn-Soldered Microdumbbell Arrays and Polyimide Films for Application to Flexible Electronics*, Intermetallics, 144, 107535.
4. Qiao, Y., Wang, Y., Tian, H., Li, M., Jian, J., Wei, Y., Tian, Y., Wang, D.-Y., Pang, Y., Geng, X., Wang, X., Zhao, Y., Wang, H., Deng, N., Jian, M., Zhang, Y., Liang, R., Yang, Y., Ren, T.-L., 2018, *Multilayer Graphene Epidermal Electronic Skin*, ACS Nano, 12(9), pp. 8839-8846.
5. Qiao, Y., Li, X., Jian, J., Wu, Q., Wei, Y., Shuai, H., Hirtz, T., Zhi, Y., Deng, G., Wang, Y., Gou, G., Xu, J., Cui, T., Tian, H., Yang, Y., Ren, T.-L., 2020, *Substrate-Free Multilayer Graphene Electronic Skin for Intelligent Diagnosis*, ACS Applied Materials & Interfaces, 12(44), pp. 49945-49956.
6. Wang, X., Dong, L., Zhang, H., Yu, R., Pan, C., Wang, Z.L., 2015, *Recent Progress in Electronic Skin*, Advanced Science, 2(10), 1500169.
7. Pu, J.-H., Zhao, X., Zha, X.-J., Bai, L., Ke, K., Bao, R.-Y., Liu, Z.-Y., Yang, M.-B., Yang, W., 2019, *Multilayer Structured Agnw/Wpu-Mxene Fiber Strain Sensors with Ultrahigh Sensitivity and a Wide Operating Range for Wearable Monitoring and Healthcare*, Journal of Materials Chemistry A, 7(26), pp. 15913-15923.
8. Duan, Z., Jiang, Y., Huang, Q., Zhao, Q., Yuan, Z., Zhang, Y., Wang, S., Liu, B., Tai, H., 2021, *Integrated Cross-Section Interface Engineering and Surface Encapsulating Strategy: A High-Response, Waterproof, and Low-Cost Paper-Based Bending Strain Sensor*, J Mater Chem C, 9(39), pp. 14003-14011.
9. Dunnill, C.W., Parkin, I.P., 2011, *Nitrogen-Doped TiO_2 Thin Films: Photocatalytic Applications for Healthcare Environments*, Dalton Transactions, 40(8), pp. 1635-1640.
10. Costa, M.S., Baptista, V., Ferreira, G.M., Lima, D., Minas, G., Veiga, M.I., Catarino, S.O., 2021, *Multilayer Thin-Film Optical Filters for Reflectance-Based Malaria Diagnostics*, Micromachines, 12(8), 890.
11. Park, H., Han, G., Lee, S.W., Lee, H., Jeong, S.H., Naqi, M., AlMutairi, A., Kim, Y.J., Lee, J., Kim, W.-j., Kim, S., Yoon, Y., Yoo, G., 2017, *Label-Free and Recalibrated Multilayer Mos2 Biosensor for Point-of-Care Diagnostics*, ACS Applied Materials & Interfaces, 9(50), pp. 43490-43497.

12. Kim, S., Lee, H., Kim, D., Ha, H., Qaiser, N., Yi, H., Hwang, B., 2020, *Ethylcellulose/Ag Nanowire Composites as Multifunctional Patchable Transparent Electrodes*, Surface and Coatings Technology, 394, 125898.
13. He, M., Wang, E., Zhang, Y., Zhang, W., Zhang, F., Zhao, C., 2020, *Performance Analysis of a Multilayer Thermoelectric Generator for Exhaust Heat Recovery of a Heavy-Duty Diesel Engine*, Applied Energy, 274, 115298.
14. Zhu, D., Beeby, S., Tudor, J., White, N., Harris, N., 2011, *Improving Output Power of Piezoelectric Energy Harvesters Using Multilayer Structures*, Procedia Engineering, 25, pp. 199-202.
15. Seo, Y., Hwang, B., 2019, *Mulberry-Paper-Based Composites for Flexible Electronics and Energy Storage Devices*, Cellulose, 26(16), pp. 8867-8875.
16. Yun, T.G., Bae, J., Rothschild, A., Kim, I.-D., 2019, *Transpiration Driven Electrokinetic Power Generator*, ACS Nano, 13(11), pp. 12703-12709.
17. Park, W., Müller, S., Baumann, R.-P., Becker, S., Hwang, B., 2020, *Surface Energy Characterization of Nanoscale Metal Using Quantitative Nanomechanical Characterization of Atomic Force Microscopy*, Applied Surface Science, 507, 145041.
18. Kozbial, A., Li, Z., Conaway, C., McGinley, R., Dhingra, S., Vahdat, V., Zhou, F., D'Urso, B., Liu, H., Li, L., 2014, *Study on the Surface Energy of Graphene by Contact Angle Measurements*, Langmuir, 30(28), pp. 8598-8606.
19. Caddeo, C., Marongiu, D., Meloni, S., Filippetti, A., Quochi, F., Saba, M., Mattoni, A., 2018, *Hydrophilicity and Water Contact Angle on Methylammonium Lead Iodide*, Advanced Materials Interfaces.
20. Sidhu, A.S., 2021, *Surface texturing of non-toxic, biocompatible titanium alloys via electro-discharge*, Reports in Mechanical Engineering, 2(1), pp. 51-56.
21. Smolin, A.Y., Filippov, A.V., Shilko, E.V., 2021, *Friction Behavior of Aluminum Bronze Reinforced by Boron Carbide Particles*, Facta Universitatis-Series Mechanical Engineering, 19(1), pp. 51-65.
22. Ha, H., Thompson, R., Matteini, P., Yoo, S.J., Hwang, B., 2022, *Effect of Surface Change by Vacuum Drying on the Sedimentation Stability of Iron Nanoparticles in Volatile Organic Solvents*, Colloid and Interface Science Communications, 48, 100625.
23. Adam, N.K., 1957, *Use of the Term 'Young's Equation' for Contact Angles*, Nature, 180(4590), pp. 809-810.
24. Kwok, D.Y., Neumann, A.W., 1999, *Contact Angle Measurement and Contact Angle Interpretation*, Advances in Colloid and Interface Science, 81(3), pp. 167-249.
25. Seveno, D., Blake, T.D., De Coninck, J., 2013, *Young's Equation at the Nanoscale*, Physical Review Letters, 111(9), 096101.
26. Niu, C., Xia, W., Peng, Y., 2018, *Analysis of Coal Wettability by Inverse Gas Chromatography and Its Guidance for Coal Flotation*, Fuel, 228, pp. 290-296.
27. Hamieh, T., 2022, *New Methodology to Study the Dispersive Component of the Surface Energy and Acid-Base Properties of Silica Particles by Inverse Gas Chromatography at Infinite Dilution*, J Chromatogr Sci, 60(2), pp. 126-142.
28. Ha, H., Ko, S., Goh, B., Müller, S., Baumann, R.-P., Leem, M., Jo Yoo, S., Choi, J., Hwang, B., 2022, *Influence of Grain Boundary Density on the Surface Energy of Nanocrystalline Metal Thin Films*, Applied Surface Science, 604, 154463.
29. Ha, H., Müller, S., Baumann, R.-P., Hwang, B., 2022, *Peakforce Quantitative Nanomechanical Imaging for Characterization of the Surface Energy of Nano-Patterned Au Strip*, Journal of Natural Fibers, 20(2), 2128150.
30. Nair, S.S., Wang, C., Wynne, K.J., 2019, *AFM Peakforce Qnm Mode for Measurement of Nanosurface Mechanical Properties of Pt-Cured Silicones*, Progress in Organic Coatings, 126, pp. 119-128.
31. Trtik, P., Kaufmann, J., Volz, U., 2012, *On the Use of Peak-Force Tapping Atomic Force Microscopy for Quantification of the Local Elastic Modulus in Hardened Cement Paste*, Cement and Concrete Research, 42(1), pp. 215-221.
32. Ning, N., Mi, T., Chu, G., Zhang, L.-Q., Liu, L., Tian, M., Yu, H.-T., Lu, Y.-L., 2018, *A Quantitative Approach to Study the Interface of Carbon Nanotubes/Elastomer Nanocomposites*, European Polymer Journal, 102, pp. 10-18.
33. Qi, Y., Jiang, D., Ju, S., Zhang, J., Cui, X., 2019, *Determining the Interphase Thickness and Properties in Carbon Fiber Reinforced Fast and Conventional Curing Epoxy Matrix Composites Using Peak Force Atomic Force Microscopy*, Composites Science and Technology, 184, 107877.
34. Derjaguin, B.V., Muller, V.M., Toporov, Y.P., 1975, *Effect of Contact Deformations on the Adhesion of Particles*, Journal of Colloid and Interface Science, 53(2), pp. 314-326.